Computer Modeling in Engineering & Sciences CMES, vol.124, no.1, pp.79-106, 2020

An Adaptive Substructure-Based Model Order Reduction Method for Nonlinear Seismic Analysis in OpenSees

Jian Wang[1, 2], Ming Fang[3, *] and Hui Li[1, 2]

Abstract: Structural components may enter an initial-elastic state, a plastic-hardening state and a residual-elastic state during strong seismic excitations. In the residual-elastic state, structural components keep in an unloading/reloading stage that is dominated by a tangent stiffness, thus structural components remain residual deformations but behave in an elastic manner. It has a great potential to make model order reduction for such structural components using the tangent-stiffness-based vibration modes as a reduced order basis. In this paper, an adaptive substructure-based model order reduction method is developed to perform nonlinear seismic analysis for structures that have a priori unknown damage distribution. This method is able to generate time-varying substructures and make nonlinear model order reduction for substructures in the residual-elastic phase. The finite element program OpenSees has been extended to provide the adaptive substructure-based nonlinear seismic analysis. At the low level of OpenSees framework, a new abstract layer is created to represent the time-varying substructures and implement the modeling process of substructures. At the high level of OpenSees framework, a new transient analysis class is created to implement the solving process of substructure-based governing equations. Compared with the conventional time step integration method, the adaptive substructure-based model order reduction method can yield comparative results with a higher computational efficiency.

Keywords: Adaptive substructure modeling, model order reduction, nonlinear seismic analysis, computer programming, OpenSees.

1 Introduction

With the rapid growth of computational capacities and simulation techniques, the finite element methods have been extensively recognized as a tool for high-fidelity simulation

[1] Key Lab of Structures Dynamic Behavior and Control of the Ministry of Education, Harbin Institute of Technology, Harbin, 150090, China.
[2] Key Lab of Smart Prevention and Mitigation of Civil Engineering Disasters of the Ministry of Industry and Information Technology, Harbin Institute of Technology, Harbin, 150090, China.
[3] College of Shipbuilding Engineering, Harbin Engineering University, Harbin, 150001, China.
* Corresponding Author: Ming Fang. Email: fangming@hrbeu.edu.cn.
Received: 18 December 2019; Accepted: 09 March 2020.

of large and complex structures. Nevertheless, it's still expensive to increase the resolution in simulations for detailed nonlinear behaviors. The model order reduction methods have drawn massive attention due to their capacity to balance accuracy and efficiency.

Model order reduction (MOR) methods basically project a full order model onto a lower dimensional space, which is spanned by a reduced order basis. According to the definitions of reduced order basis, the MOR methods are classified as the proper orthogonal decomposition (POD) [Kerschen and Golinval (2002); Chatterjee (2000); Kerschen, Golinval, Vakakis et al. (2005)], proper generalized decomposition (PGD) [Ladevèze, Passieux and Néron (2010); Chinesta, Ammar and Cueto (2010); Nouy (2010)], reduced basis (RB) method [Hesthaven, Rozza and Stamm (2016); Quarteroni, Manzoni and Negri (2016); Rozza, Huynh and Patera (2007); Grepl (2005)], component mode synthesis (CMS) [Hurty (1963); Bampton and Craig (1968)], and machine learning approaches [Mohamed (2018); Moosavi, Stefanescu and Sandu (2015)], etc. Such projection-based MOR methods have gained mature application in linear systems and achieved major computational savings. During recent decades, these projection-based MOR methods were also advanced to cope with nonlinear systems and encourage application in large and complex structures.

The POD constructs the reduced order basis in an a posteriori manner through directly solving the original problem. While the PGD generates the reduced order basis in an a priori manner using an iteration algorithm. Starting from the POD and PGD techniques, a group of methods are triggered to reduce the dimension of nonlinear systems, such as Discrete Empirical Interpolation method [Chaturantabut and Sorensen (2010); Aguado, Chinesta, Leygue et al. (2013)], Hyper reduction method [Ryckelynck (2009); Amsallem, Zahr and Farhat (2012)], and Gauss Newton with Approximation Tensor method [Carlberg, Farhat, Cortial et al. (2012); Farhat, Avery, Chapman et al. (2014)]. Recently, the POD has been incorporated with domain decomposition methodology for the dynamic analysis of elastic-plastic structural problems [Corigliano, Dossi and Mariani (2015)]. And the PGD has incorporated with the Reference Point Method to construct the reduced order model of a nonlinear problem [Capaldo, Guidault, Néron et al. (2017)]. On the other side, the RB method makes model order reduction by carrying out an offline-online framework. The offline stage takes responsibility for selecting the reduced basis functions, and the online stage is in charge of obtaining the coefficients of the reduced basis functions. The RB method has been advanced to deal with nonlinear issues, such as the Reduced-Basis-Element Method [Maday and Rønquist (2002, 2005)], Static-Condensation Reduced-Basis-Element method [Huynh, Knezevic and Patera (2013a, 2013b); Vallaghé and Patera (2014)], etc. The RB method recently integrated the machine learning method to treat nonlinear problems in the online stage [Guo and Hesthaven (2018)]. Taking advantage of machine learning, regression-based methods for model order reduction have applied to nonlinear problems, such as artificial neural networks [Moosavi, Stefanescu and Sandu (2015)] and the Gaussian process regression [Nguyen and Peraire (2016)]. As a substructure-based MOR method, the CMS method

partitions the finite element model into a set of substructures, and selects a small number of substructure modes as reduced order bases to capture the dominant vibration characteristics. The CMS method has also been applied to model order reduction for nonlinear dynamic models, such as nonlinear landing simulation of aircraft system [He, Wang and Chen (2016)], soil-structure interaction simulation [Wang and Jiang (2012)], etc.

For nonlinear seismic analysis of civil structures, structural components in plastic regime are usually sparsely distributed. The CMS method has a great advantage to simulate the sparsely distributed damage. Because the entire structure is divided into linear and nonlinear substructures, and the degrees of freedoms (DOFs) of linear substructures can be substantially condensed by reduced order bases. Nevertheless, the distribution of damaged structural components is a priori unknown because of the randomness of seismic excitations. Thus the linear-nonlinear interface can't be determined in advance. To cope with the issue, the authors have previously proposed an adaptive substructure modeling strategy [Fang, Wang and Li (2018)] that integrated the CMS method to simulate tall buildings with a priori unknown damage distribution. One issue limits the application of the previously proposed method. When the ground motion intensity increases to a strong nonlinear level, the distribution of damaged structural components expands spatially, which results in a small portion of linear substructures and a large portion of nonlinear substructures. The MOR effect is lowered for linear substructures. Therefore, it's considerably essential to develop an adaptive substructure-based MOR method that considers both the adaptive substructure modeling and nonlinear model order reduction.

The substructure-based MOR method has already been implemented in commercial finite element (FE) programs, such as ABAQUS [ABAQUS (2019)] and ANSYS [ANSYS (2019)], etc. The substructure modeling techniques in these programs require the prior-prescribed linear-nonlinear interface, which is unable to simulate time-varying substructures during the seismic loading period. Meanwhile, the flexibility and extensibility of commercial FE programs are usually limited to a few user-defined materials or elements. Thus it's recommended to implement the adaptive substructure-based MOR method in an open source program for nonlinear seismic analysis. In the last two decades, OpenSees [Mckenna, Scott and Fenves (2010)] has become one of the most popular programs for numerical simulation of earthquake engineering due to its great flexibility and extensibility. The architecture of OpenSees is designed according to the software design pattern provided by Gamma et al. [Gamma, Helm, Johnson et al. (1995)], which is organized with the ability to sustainably integrate the newest research outcomes. For instance, the OpenSees has incorporated with peridynamic theory to simulate discontinuous problems in civil engineering, such as concrete cracks [Gu, Wang and Huang (2019); Sun, Li, Gu et al. (2019)]. And the OpenSees has been advanced with high-performance triangular shell element and explicit algorithm for strong nonlinear analysis [Lu, Tian, Sun et al. (2019); Lu, Xie, Guan et al. (2015)]. It's believed that the OpenSees architecture is suitable for implementing the adaptive substructure-based MOR method.

The objective of this paper is to develop an adaptive substructure-based MOR method with the capacity of nonlinear model order reduction, and implement this method in OpenSees for nonlinear seismic analysis. During an earthquake excitation, structural components may undergo the initial-elastic state, the plastic-hardening state, and the residual-elastic state. In the residual-elastic state, the residual deformation remains and structural components behave in an elastic manner. An adaptive substructure modeling strategy has incorporated with substructure-based MOR methods to make DOF reduction in each phase. A new abstract layer of substructure and a new transient analysis class are created to implement the modeling process of substructures and the solving process of substructure-based governing equations, respectively. Some existing classes are modified, so as to merge the new classes with the original software architecture. The numerical performance is tested through a nonlinear RC structure subjected to seismic excitations.

In Section 2, the adaptive substructure modeling strategy is introduced, and the substructure-based MOR methods in three types of phase are deduced. In Section 3, the implementation of the adaptive substructure-based MOR method is described using the graphical Unified Modeling Language notation. In Section 4, the accuracy and efficiency are tested using a 12-story RC frame structure under seismic excitations. Section 5 summarizes the conclusions of the investigation.

2 Adaptive substructure-based MOR method

During the strong seismic excitation, damaged structural components are distributed sparsely in general, and the damage distribution expands spatially as the input acceleration amplitude increases. To accelerate the nonlinear seismic analysis, the substructure-based MOR method is employed for FE simulation due to its flexible substructure modeling for sparse damage distribution. Meanwhile an adaptive substructure modeling strategy is developed to adjust the MOR method to the gradually expanding damage distribution. It means the substructure modeling should be time-varying as the damage distribution is changing during the seismic loading period. The whole seismic loading period is classified as three types of phase, i.e., the initial-elastic phase, the plastic-hardening phase and the residual-elastic phase. The adaptive substructure-based model order reduction (AMOR) method utilize an adjustable substructure modeling strategy and substructure-based MOR approaches during each type of phase. Fig. 1 shows the flowchart of the AMOR method.

The governing equation of a nonlinear structure can be formulated as Eq. (1)

$$\mathbf{M}_g\ddot{\mathbf{u}}_g+\mathbf{C}_g\underline{\mathbf{u}}_g+\mathbf{K}_g\mathbf{u}_g+\mathbf{R}(\mathbf{u}_g,\dot{\mathbf{u}}_g)=\mathbf{f}_g \tag{1}$$

where $\mathbf{M}_g$, $\mathbf{C}_g$ and $\mathbf{K}_g$ are the mass, damping, and stiffness matrices, respectively; $\mathbf{R}(\mathbf{u}_g,\dot{\mathbf{u}}_g)$ and $\mathbf{f}_g$ are the nonlinear restoring force vector and external force vectors, respectively. $\mathbf{u}_g$ is the displacement vector. The subscript 'g' denotes the global DOFs of the nonlinear structure. The substructure-based MOR approaches are developed for Eq. (1) during different phases, and the formulation are introduced as follows.

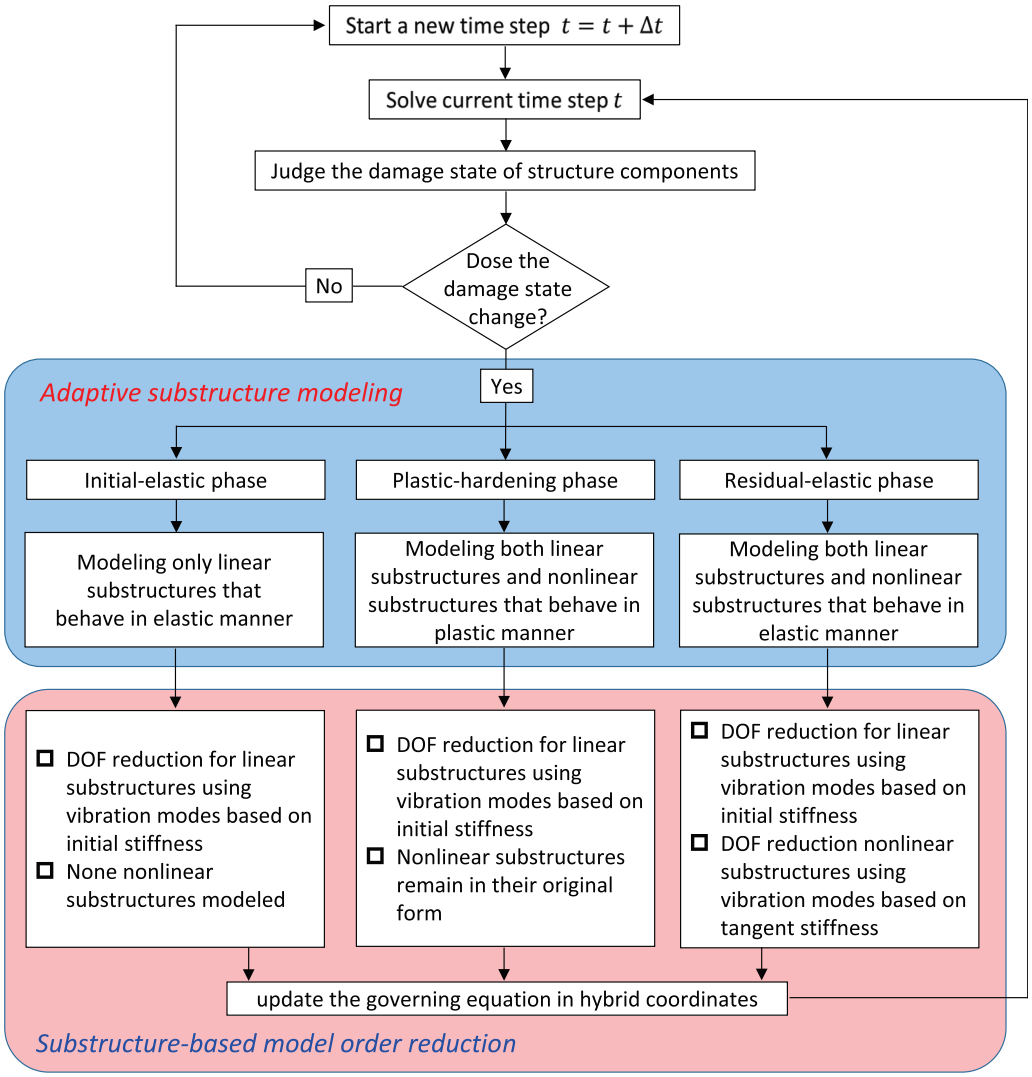

Figure 1: Flowchart of the adaptive model order reduction method

2.1 Initial-elastic phase

At the initial period of seismic loads, all structural components keep elastic due to the low input acceleration amplitudes. This period is considered to be the initial-elastic phase.

Since the whole structure is initially elastic, the governing equation can be formulated using a few modal coordinates as follows:

$$\mathbf{M}_d^e \ddot{\mathbf{q}}_d^e + \mathbf{C}_d^e \dot{\mathbf{q}}_d^e + \mathbf{K}_d^e \mathbf{q}_d^e = \mathbf{f}_d^e \tag{2}$$

where $\mathbf{M}_d^e=\mathbf{\Phi}_d^T\mathbf{M}_g\mathbf{\Phi}_d$, $\mathbf{C}_d^e=\mathbf{\Phi}_d^T\mathbf{C}_g\mathbf{\Phi}_d$, $\mathbf{K}_d^e=\mathbf{\Phi}_d^T\mathbf{K}_g\mathbf{\Phi}_d$, $\mathbf{f}_d^e=\mathbf{\Phi}_d^T\mathbf{f}_g$ are the mass, damping, stiffness matrices and external load vector in the modal coordinate space, respectively. $\mathbf{\Phi}_d$ is the dominant vibration modes that are selected as a set of reduced bases. $\mathbf{q}_d^e$ is the corresponding displacement coordinates in modal coordinate space. The subscript 'd' represents the modal coordinate space that is constructed using dominant vibration modes. The superscript 'e' represents the initial-elastic phase.

In the governing equation Eq. (2), the seismic response is obtained through the superposition of dominant vibration modes. Normally, a small number of vibration modes are able to simulate the dynamic response of the structure under seismic excitation. Thus the FE model DOFs can be reduced substantially for large and complex structures, and the nonlinear seismic analysis during the initial-elastic phase is remarkably accelerated.

2.2 Plastic-hardening phase

After the initial-elastic phase, the input acceleration amplitude increases and yield a larger structural deformation. For severe ground shakings, structural components may enter an inelastic phase, during which the plastic strain increase and cause strain hardening in constitutive models. This period is considered to be the plastic-hardening phase.

Once structural components enter nonlinear stage, the displacement vector $\mathbf{u}_g$ is partitioned into three sub-vectors, i.e., $\mathbf{u}_g=\{\mathbf{u}_l \quad \mathbf{u}_b \quad \mathbf{u}_n\}^T$. The subscripts 'l', 'b' and 'n' stands for the DOFs inside the linear substructures, on the linear-nonlinear interface and inside the nonlinear substructures, respectively. The model order reduction is made only for linear substructures, while the linear-nonlinear interface and the nonlinear substructures remain in their original form. And the DOF reduction is conducted through the coordinate space transformation. The displacement vector is transformed from the physical coordinate space to the hybrid coordinate space as Eq. (3):

$$\begin{Bmatrix}\mathbf{u}_l\\ \mathbf{u}_b\\ \mathbf{u}_n\end{Bmatrix}\approx\begin{bmatrix}\bar{\mathbf{\Phi}}_d & \bar{\mathbf{\Psi}}_b & \mathbf{0}\\ \mathbf{0} & \mathbf{I}_b & \mathbf{0}\\ \mathbf{0} & \mathbf{0} & \mathbf{I}_n\end{bmatrix}\begin{Bmatrix}\mathbf{q}_l^p\\ \mathbf{u}_b^p\\ \mathbf{u}_n^p\end{Bmatrix} \tag{3}$$

where $\bar{\mathbf{\Phi}}_d$ is the selected vibration modes of linear substructures, and $\bar{\mathbf{\Psi}}_b$ is the constraint modes of linear substructures. $\mathbf{I}_b$ and $\mathbf{I}_n$ are both identity matrices. $\mathbf{q}_l^p$ is the displacement vector of linear substructures in modal coordinate space, while the sub-vector $\mathbf{u}_b^p$ and $\mathbf{u}_n^p$ remain unchanged in physical coordinate space. The superscript 'p' stands for the plastic-hardening phase. Thus the governing equation is formulated in hybrid coordinate space as Eq. (4).

$$\mathbf{M}_h^p\ddot{\mathbf{u}}_h^p+\mathbf{C}_h^p\dot{\mathbf{u}}_h^p+\mathbf{K}_h^p\mathbf{u}_h^p+\mathbf{R}_h^p=\mathbf{f}_h^p \tag{4}$$

where

$$\mathbf{M}_h^p=\begin{bmatrix}\bar{\boldsymbol{\Phi}}_d^T\mathbf{M}_{ll}\bar{\boldsymbol{\Phi}}_d & \bar{\boldsymbol{\Phi}}_d^T\mathbf{M}_{ll}\bar{\boldsymbol{\Psi}}_b & \mathbf{0}\\ \bar{\boldsymbol{\Psi}}_b^T\mathbf{M}_{ll}\bar{\boldsymbol{\Phi}}_d & \bar{\boldsymbol{\Psi}}_b^T\mathbf{M}_{ll}\bar{\boldsymbol{\Psi}}_b+\mathbf{M}_{bb} & \mathbf{0}\\ \mathbf{0} & \mathbf{0} & \mathbf{M}_{nn}\end{bmatrix},\ \mathbf{K}_h^p=\begin{bmatrix}\bar{\boldsymbol{\Phi}}_d^T\mathbf{K}_{ll}\bar{\boldsymbol{\Phi}}_d & \mathbf{0} & \mathbf{0}\\ \mathbf{0} & \mathbf{K}_{bb}-\mathbf{K}_{bl}\mathbf{K}_{ll}^{-1}\mathbf{K}_{lb} & \mathbf{K}_{bn}\\ \mathbf{0} & \mathbf{K}_{nb} & \mathbf{K}_{nn}\end{bmatrix},$$

$$\mathbf{C}_h^p=\begin{bmatrix}\bar{\boldsymbol{\Phi}}_d^T\mathbf{C}_{ll}\bar{\boldsymbol{\Phi}}_d & \bar{\boldsymbol{\Phi}}_d^T(\mathbf{C}_{ll}\bar{\boldsymbol{\Psi}}_b+\mathbf{C}_{lb}) & \mathbf{0}\\ (\bar{\boldsymbol{\Psi}}_b^T\mathbf{C}_{ll}+\mathbf{C}_{bl})\bar{\boldsymbol{\Phi}}_d & \bar{\boldsymbol{\Psi}}_b^T\mathbf{C}_{ll}\bar{\boldsymbol{\Psi}}_b+\mathbf{C}_{bl}\bar{\boldsymbol{\Psi}}_b+\bar{\boldsymbol{\Psi}}_b^T\mathbf{C}_{lb}+\mathbf{C}_{bb} & \mathbf{C}_{bn}\\ \mathbf{0} & \mathbf{C}_{nb} & \mathbf{C}_{nn}\end{bmatrix}$$

$$\mathbf{R}_h^p=\begin{Bmatrix}\mathbf{0}\\ \mathbf{0}\\ \mathbf{R}_n(\mathbf{u}_n,\dot{\mathbf{u}}_n)\end{Bmatrix},\ \mathbf{u}_h^p=\begin{Bmatrix}\mathbf{q}_l^p\\ \mathbf{u}_b^p\\ \mathbf{u}_n^p\end{Bmatrix},\ \mathbf{f}_h^p=\begin{Bmatrix}\bar{\boldsymbol{\Phi}}_d^T\mathbf{f}_l\\ \bar{\boldsymbol{\Psi}}_b^T\mathbf{f}_l+\mathbf{f}_b\\ \mathbf{f}_n\end{Bmatrix}$$

$\mathbf{u}_h^p$ is the displacement vector in the hybrid coordinate space. $\mathbf{R}_h^p$ is the nonlinear restoring force vector. The subscript 'h' represents the hybrid coordinate space that is composed of physical coordinates and modal coordinates.

In the governing equation Eq. (4), the seismic response of linear substructures is obtained using the superposition of dominant modes, while the interface and the nonlinear substructures still remain in physical coordinate space without DOF reduction. Such a DOF reduction method will achieve great computational savings when the proportion of linear DOFs is large and the number of selected substructure modes is small. When new structural components enter nonlinear stage, the linear and nonlinear substructures are remodeled and the partition of displacement vectors in Eqs. (3) and (4) is updated.

2.3 Residual-elastic phase

After the plastic-hardening phase, the severe shaking is attenuated and input acceleration amplitudes drop back to a low level. Structural components keep in an unloading/reloading stage that is dominated by a tangent stiffness. Thus Structural components remain residual deformations but behave in an elastic manner. This period is considered to be a residual-elastic phase.

In the residual-elastic phase, the governing equation is represented in an incremental form. The displacement vector of nonlinear substructures $\mathbf{u}_n$ is calculated by a summation of the response at the previous time step and an elastically incremental response $\Delta\mathbf{u}_n$ at the current time step. The incremental displacement vector $\Delta\mathbf{u}_n$ is transformed from the physical coordinate space to the modal coordinate space that is spanned by tangent-stiffness-based vibration modes. Thus the incremental displacement vector is formulated as Eq. (5).

$$\begin{Bmatrix}\Delta\mathbf{u}_l\\ \Delta\mathbf{u}_b\\ \Delta\mathbf{u}_n\end{Bmatrix}\approx\begin{bmatrix}\bar{\boldsymbol{\Phi}}_d & \bar{\boldsymbol{\Psi}}_b & \mathbf{0}\\ \mathbf{0} & \mathbf{I}_{bb} & \mathbf{0}\\ \mathbf{0} & \tilde{\boldsymbol{\Psi}}_b & \tilde{\boldsymbol{\Phi}}_d\end{bmatrix}\begin{Bmatrix}\Delta\mathbf{q}_l^{er}\\ \Delta\mathbf{u}_b^{er}\\ \Delta\mathbf{q}_n^{er}\end{Bmatrix}\tag{5}$$

where $\tilde{\mathbf{\Phi}}_d$ is the selected vibration modes of nonlinear substructures, and $\tilde{\mathbf{\Psi}}_b$ is the constraint modes of nonlinear substructures. It's noted that $\tilde{\mathbf{\Phi}}_d$ is calculated using the tangent stiffness of nonlinear substructures. $\Delta\mathbf{q}_l^{er}$ and $\Delta\mathbf{q}_n^{er}$ are the incremental displacement of the linear and nonlinear substructures in modal coordinate space, respectively. The superscript 'er' represents the residual-elastic phase. Thus the governing equation is formulated in an incremental form as follows.

$$\mathbf{M}_h^{er}\Delta\ddot{\mathbf{u}}_h^{er}+\mathbf{C}_h^{er}\Delta\dot{\mathbf{u}}_h^{er}+\mathbf{K}_h^{er}\Delta\mathbf{u}_h^{er}=\Delta\mathbf{f}_h^{er} \tag{6}$$

where

$$\mathbf{M}_h^{er}=\begin{bmatrix} \bar{\mathbf{\Phi}}_d^T\mathbf{M}_{ll}\bar{\mathbf{\Phi}}_d & \bar{\mathbf{\Phi}}_d^T\mathbf{M}_{ll}\bar{\mathbf{\Psi}}_b & \mathbf{0} \\ \bar{\mathbf{\Psi}}_b^T\mathbf{M}_{ll}\bar{\mathbf{\Phi}}_d & \bar{\mathbf{\Psi}}_b^T\mathbf{M}_{ll}\bar{\mathbf{\Psi}}_b+\mathbf{M}_{bb}+\tilde{\mathbf{\Psi}}_b^T\mathbf{M}_{nn}\tilde{\mathbf{\Psi}}_b & \tilde{\mathbf{\Psi}}_b^T\mathbf{M}_{nn}\tilde{\mathbf{\Phi}}_d \\ \mathbf{0} & \tilde{\mathbf{\Phi}}_d^T\mathbf{M}_{nn}\tilde{\mathbf{\Psi}}_b & \tilde{\mathbf{\Phi}}_d^T\mathbf{M}_{nn}\tilde{\mathbf{\Phi}}_d \end{bmatrix},$$

$$\mathbf{K}_h^{er}=\begin{bmatrix} \bar{\mathbf{\Phi}}_d^T\mathbf{K}_{ll}\bar{\mathbf{\Phi}}_d & \mathbf{0} & \mathbf{0} \\ \mathbf{0} & \mathbf{K}_{bb}-\mathbf{K}_{bl}\mathbf{K}_{ll}{}^{-1}\mathbf{K}_{lb}-\mathbf{K}_{bn}\mathbf{K}_{nn}{}^{-1}\mathbf{K}_{nb} & \mathbf{0} \\ \mathbf{0} & \mathbf{0} & \tilde{\mathbf{\Phi}}_d^T\mathbf{K}_{nn}\tilde{\mathbf{\Phi}}_d \end{bmatrix},$$

$$\mathbf{C}_h^{er}=\begin{bmatrix} \bar{\mathbf{\Phi}}_d^T\mathbf{C}_{ll}\bar{\mathbf{\Phi}}_d & \bar{\mathbf{\Phi}}_d^T(\mathbf{C}_{ll}\bar{\mathbf{\Psi}}_b+\mathbf{C}_{lb}) & \mathbf{0} \\ (\bar{\mathbf{\Psi}}_b^T\mathbf{C}_{ll}+\mathbf{C}_{bl})\bar{\mathbf{\Phi}}_d & \begin{pmatrix}\bar{\mathbf{\Psi}}_b^T\mathbf{C}_{ll}\bar{\mathbf{\Psi}}_b+\mathbf{C}_{bl}\bar{\mathbf{\Psi}}_b+\bar{\mathbf{\Psi}}_b^T\mathbf{C}_{lb}+\mathbf{C}_{bb} \\ +\tilde{\mathbf{\Psi}}_b^T\mathbf{C}_{nn}\tilde{\mathbf{\Psi}}_b+\mathbf{C}_{bn}\tilde{\mathbf{\Psi}}_b+\bar{\mathbf{\Psi}}_b^T\mathbf{C}_{nb}\end{pmatrix} & (\tilde{\mathbf{\Psi}}_b^T\mathbf{C}_{nn}+\mathbf{C}_{bn})\tilde{\mathbf{\Phi}}_d \\ \mathbf{0} & \bar{\mathbf{\Phi}}_d^T(\mathbf{C}_{nn}\tilde{\mathbf{\Psi}}_b+\mathbf{C}_{nb}) & \bar{\mathbf{\Phi}}_d^T\mathbf{C}_{nn}\bar{\mathbf{\Phi}}_d \end{bmatrix}$$

$$\Delta\mathbf{f}_h^{er}=\begin{Bmatrix} \bar{\mathbf{\Phi}}_d^T\Delta\mathbf{f}_l \\ \bar{\mathbf{\Psi}}_b^T\Delta\mathbf{f}_l+\Delta\mathbf{f}_b+\tilde{\mathbf{\Psi}}_b^T\Delta\mathbf{f}_n \\ \tilde{\mathbf{\Phi}}_d^T\Delta\mathbf{f}_n \end{Bmatrix},\ \Delta\mathbf{u}_h^{er}=\begin{Bmatrix} \Delta\mathbf{q}_l^{er} \\ \Delta\mathbf{u}_b^{er} \\ \Delta\mathbf{q}_n^{er} \end{Bmatrix}$$

In the governing equation Eq. (6), the seismic response of linear substructures is obtained using the superposition of vibration modes based on initial stiffness, while nonlinear substructures are simulated through the superposition of tangent-stiffness-based vibration modes. Only the substructure interface remains in its original form without DOF reduction. When the acceleration amplitude drops down to low level after severe ground shakings, such a MOR method will surely achieve a further DOF reduction. The Eq. (6) is solved during the residual-elastic phase before new damaged structural components arise, or existing damaged structural components return to the plastic-hardening phase. The plastic-hardening phase and residual-elastic phase will alternate with each other until the end of seismic excitations.

2.4 AMOR algorithm

In order to proceed the AMOR analysis, the Newton-Raphson method is utilized to solve the abovementioned governing equations by conducting an iterative solution procedure, and the

Newmak-β integration method is employed. The processing steps of the AMOR algorithm is summarized as below.

Step 1: Initial preparation (t=0)

a) $\mathbf{M}_g$, $\mathbf{C}_g$, $\mathbf{K}_g$ and $\mathbf{f}_g$ are given.
b) The whole structure initially elastic and Eq. (2) is constructed.
c) Time interval Δt is determined.
d) Parameters γ and β are determined in the Newmak-β method.
e) Determine the maximum iteration number $i_{\max}$.

Step 2: Start a new time step: t=t+Δt

a) Initialize iteration number i=0
b) Use direct integration method to determine the trial values $\left\{\mathbf{u}_{g_{t+\Delta t}}^{(0)}, \dot{\mathbf{u}}_{g_{t+\Delta t}}^{(0)}, \ddot{\mathbf{u}}_{g_{t+\Delta t}}^{(0)}\right\}$
c) If. (Initial-elastic phase)

Values $\left\{\mathbf{u}_{g_{t+\Delta t}}^{(0)}, \dot{\mathbf{u}}_{g_{t+\Delta t}}^{(0)}, \ddot{\mathbf{u}}_{g_{t+\Delta t}}^{(0)}\right\}$ are transformed to $\left\{\mathbf{q}_{d_{t+\Delta t}}^{(0)}, \dot{\mathbf{q}}_{d_{t+\Delta t}}^{(0)}, \ddot{\mathbf{q}}_{d_{t+\Delta t}}^{(0)}\right\}$ in modal coordinates using matrix $\mathbf{\Phi}_d$.

Else.

Values $\left\{\mathbf{u}_{g_{t+\Delta t}}^{(0)}, \dot{\mathbf{u}}_{g_{t+\Delta t}}^{(0)}, \ddot{\mathbf{u}}_{g_{t+\Delta t}}^{(0)}\right\}$ are transformed to $\left\{\mathbf{u}_{h_{t+\Delta t}}^{(0)}, \dot{\mathbf{u}}_{h_{t+\Delta t}}^{(0)}, \ddot{\mathbf{u}}_{h_{t+\Delta t}}^{(0)}\right\}$ in hybrid coordinates using matrix in Eqs. (3) or (5).

Step 3: Solve current time Step

a) Determine generalized tangent matrix

If. (Initial-elastic phase) $\tilde{\mathbf{K}}_{d_{t+\Delta t}}^{(i)} = \dfrac{1}{\beta\Delta t^2}\mathbf{M}_{d_{t+\Delta t}} + \dfrac{\gamma}{\beta\Delta t}\mathbf{C}_{d_{t+\Delta t}} + \mathbf{K}_{d_{t+\Delta t}}$

Else. $\tilde{\mathbf{K}}_{h_{t+\Delta t}}^{(i)} = \dfrac{1}{\beta\Delta t^2}\mathbf{M}_{h_{t+\Delta t}} + \dfrac{\gamma}{\beta\Delta t}\mathbf{C}_{h_{t+\Delta t}} + \mathbf{K}_{h_{t+\Delta t}} + \left.\dfrac{\partial \mathbf{R}_h}{\partial \mathbf{u}_{h_{t+\Delta t}}}\right|_{\mathbf{u}_{h_{t+\Delta t}}^{(i)}} + \dfrac{\gamma}{\beta\Delta t}\left.\dfrac{\partial \mathbf{R}_h}{\partial \underline{\mathbf{u}}_{h_{t+\Delta t}}}\right|_{\underline{\mathbf{u}}_{h_{t+\Delta t}}^{(i)}}$

b) Determine generalized unbalance vector

If. (Initial-elastic phase) $\tilde{\mathbf{P}}_{d_{t+\Delta t}}^{(i)} = \mathbf{f}_{d_{t+\Delta t}} - \mathbf{M}_{d_{t+\Delta t}}\ddot{\mathbf{u}}_{d_{t+\Delta t}}^{(i)} - \mathbf{C}_{d_{t+\Delta t}}\dot{\mathbf{q}}_{d_{t+\Delta t}}^{(i)} - \mathbf{K}_{d_{t+\Delta t}}\mathbf{q}_{d_{t+\Delta t}}^{(i)}$

Else. $\tilde{\mathbf{P}}_{h_{t+\Delta t}}^{(i)} = \mathbf{f}_{h_{t+\Delta t}} - \mathbf{M}_{h_{t+\Delta t}}\ddot{\mathbf{u}}_{h_{t+\Delta t}}^{(i)} - \mathbf{C}_{h_{t+\Delta t}}\dot{\mathbf{u}}_{h_{t+\Delta t}}^{(i)} - \mathbf{K}_{h_{t+\Delta t}}\mathbf{u}_{h_{t+\Delta t}}^{(i)} - \mathbf{R}_h(\mathbf{u}_{h_{t+\Delta t}}^{(i)}, \dot{\mathbf{u}}_{h_{t+\Delta t}}^{(i)})$

c) Solve the generalized equilibrium equation.

If. (Initial-elastic phase) $\tilde{\mathbf{K}}_{d_{t+\Delta t}}^{(i)}(\mathbf{q}_{d_{t+\Delta t}} - \mathbf{q}_{d_{t+\Delta t}}^{(i)}) = \tilde{\mathbf{P}}_{d_{t+\Delta t}}^{(i)}$

Else. $\tilde{\mathbf{K}}_{h_{t+\Delta t}}^{(i)}(\mathbf{u}_{h_{t+\Delta t}} - \mathbf{u}_{h_{t+\Delta t}}^{(i)}) = \tilde{\mathbf{P}}_{h_{t+\Delta t}}^{(i)}$

d) Transform the displacement vector to $\mathbf{u}_{g_{t+\Delta t}}$ in physical coordinates.
e) Convergence test.
f) If. (solution is converged) go to Step 4
Else if. ($i > i_{\max}$) fail to converge and go to the Step 8.
Else start a new iteration: i=i+1 and go to Step 3(a)

Step 4: Check damage state

a) Check the damage state of all structural components. If damage state changes, go to Step 5; otherwise go to Step 7.

Step 5: Adaptive substructure modeling

a) If the structural components are in the initial-elastic phase, model them as linear substructures that behave in elastic manner.
b) If the structural components are in the plastic-hardening phase, model them as nonlinear substructures that behave in plastic manner.
c) If the structural components are in the residual-elastic phase, model them as nonlinear substructures that behave in elastic manner.

Step 6: update the governing equation in hybrid coordinates.

a) If Step 5(a) is reached, make DOF reduction for linear substructures using vibration modes based on initial stiffness. Eq. (2) is constructed.
b) If Step 5(b) is reached, make DOF reduction for linear substructures using vibration modes based on initial stiffness, while nonlinear substructures remain in their original form. Eq. (4) is constructed.
c) If Step 5(c) is reached, make DOF reduction for linear substructures using vibration modes based on initial stiffness, while make DOF reduction for nonlinear substructures using vibration modes based on tangent stiffness. Eq. (6) is constructed.
d) Go back to Step 3(a).

Step 7: Submit the solution

a) Commit the converged displacement values.
b) If it's not the last time step, go to Step 2; otherwise go the Step 8.

Step 8: END

3 AMOR implementation in OpenSees

Implementation of the AMOR method requires program modifications over class inheritance at both the low level and the high level of OpenSees framework. At the low level of OpenSees framework, a ModelBuilder object populates the objects of the nodes, elements, constraints and load patterns of a FE model through an input script. All the objects created by the ModelBuilder compose a Domain object. At the high level of OpenSees framework, the state of each domain component is computed by an Analysis object, which is composed of constraint handler, time integrator, solution algorithm, storage of equation and equation solver, etc. To avoid tight coupling of domain components and the analysis methods, the OpenSees framework provides a layer of abstraction between objects in the domain and the governing equations. This layer of abstraction is defined as an AnalysisModel object. However, the implementation of AMOR

method requires a substructure-based layer of abstraction to achieve the substructure modeling and substructure-based model order reduction. The DOF reduction of substructures involves two numerical procedures: the mode calculation and selection, and the assembly of governing equations in hybrid coordinate space. Significantly, the AMOR analysis has been implemented with a reanalysis ability to gradually changing the substructure modeling pattern according to the time-varying structural damage distribution. The class diagram of the AMOR implementation in OpenSees is shown in Fig. 2.

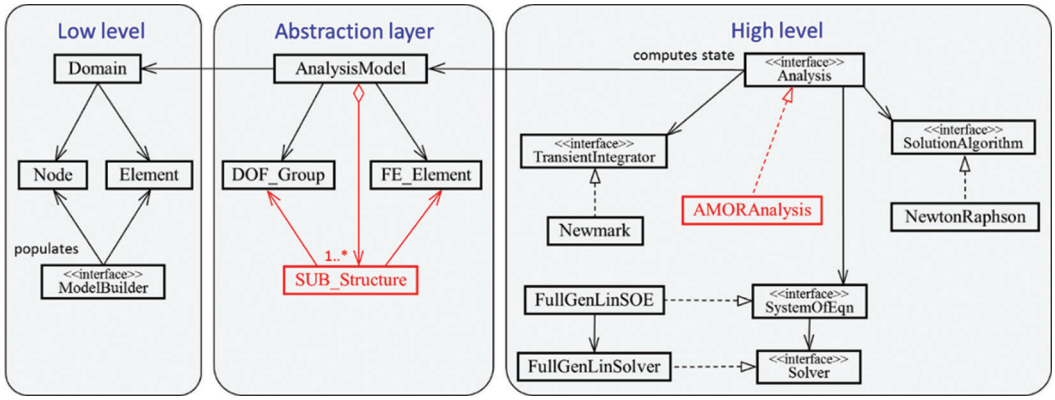

Figure 2: Class diagram of the AMOR implementation in OpenSees

3.1 Substructure-based abstraction layer

The implementation of substructure-based abstraction layer includes substructure partitioning and substructure numbering. The substructure partitioning is based on the topology relation of structural components, while the substructure numbering maps the substructure DOFs and governing equations.

3.1.1 Substructure modeling

For a given time step during a nonlinear seismic analysis, the damage states of structural components are determined by their deformation at the previous time step. A pair of structural components are recognized as two vertices connected by an edge in topology relation, if they are adjacent and keep in the same damage state. Linear and nonlinear substructures are both aggregations of a set of structural components that share the same damage states. Obviously, each substructure is surrounded by other substructures with different damage states. The class diagram of partitioning substructures is illustrated in Fig. 3(a). The SUB_Structure class is the additional layer of abstraction between the AnalysisModel and its component objects. The SUB_Structure is created to provide a middle-level component object in AnalysisModel and present the linear and nonlinear substructures in a FE model. The method partitionSubs() in AnalysisModel is defined to generate SUB_Structure objects and partition linear and nonlinear substructures based on the topology relation of structural components. Each SUB_Structure can access the nodes

and elements within it through calling the functions getDOF_GroupIter() and getFE_ElementIter(), respectively.

3.1.2 Substructure partitioning

Once the substructures are modeled, the substructures are numbered one by one and the numbering process of each substructure is independent from other substructures. The internal DOFs of each substructure are numbered individually, and the resulting DOF numbers are utilized to calculated substructure modes. The shared interface DOFs of adjacent substructures are numbered together, and keep their DOF numbers unchanged in the governing equations. The class diagram of partitioning and numbering substructures is illustrated in Fig. 3(b). The number_Substructures() and number_Equations() are defined in DOF_Numberer to accomplish the DOF numbering process. The method number_Substructure() numbers the internal DOFs of substructures, and the numbering results are prepared for the mode calculation and selection of substructures. Meanwhile,

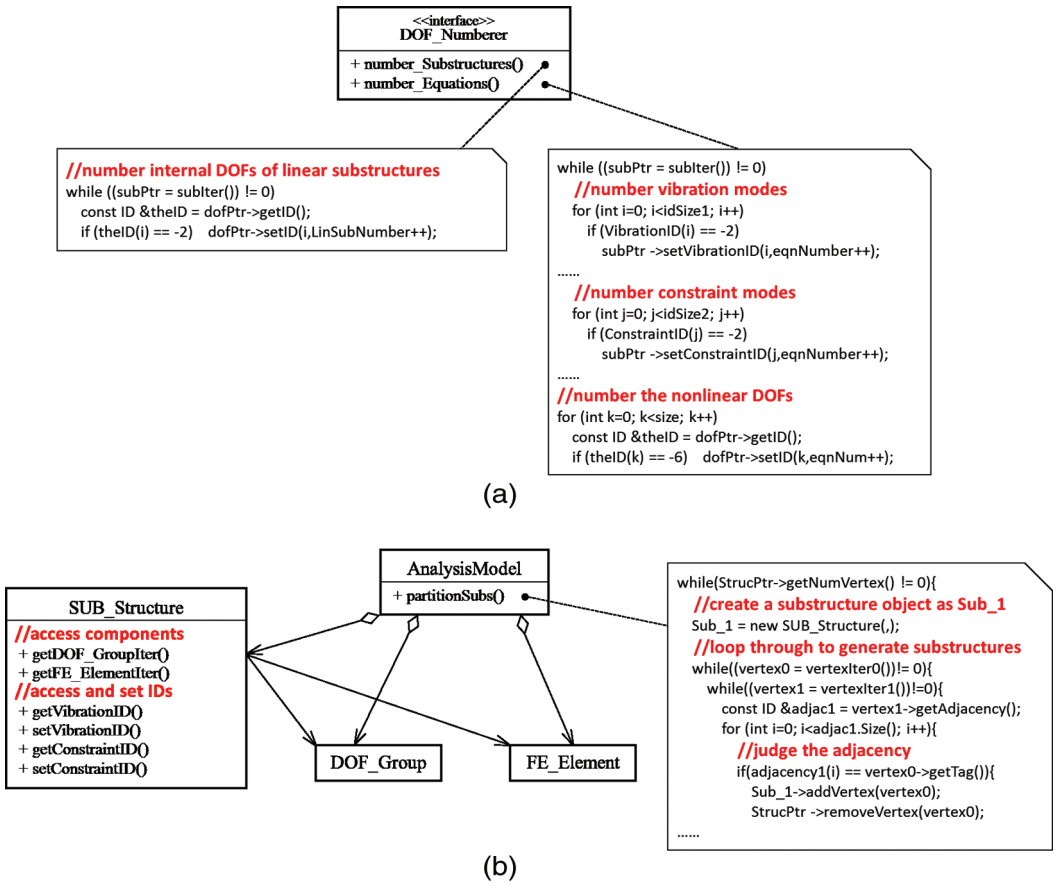

Figure 3: Class diagram of partitioning and numbering substructures

the method number_Equations() is responsible for numbering the governing equations in hybrid coordinates, which includes numbering the vibration modes, constraint modes of linear substructures and the nonlinear DOFs.

3.2 Substructure-based model order reduction

3.2.1 Mode calculation and selection

The implementation of mode calculation involves solving vibration modes and constraint modes of substructures. The vibration modes are extracted from solving the eigen equations for substructures. The eigen equations are based on initial stiffness for linear substructures and based on tangent stiffness for nonlinear substructures. The constraint modes are obtained through the implementation of the Guyan reduction method [Guyan (1965)]. On the other side, the mode selection has only been made for the vibration modes of substructures. During the initial-elastic period, the effective modal mass is utilized to rank the importance of vibration modes of the entire structure. During the plastic-hardening period and residual-elastic period, the effective interface mass is employed to evaluate the contribution of vibration modes to the dynamic response of substructures. The effective interface mass [Kammer and Triller (1996)] measures the contribution of each vibration mode to the internal loads at the interface. And a larger effective interface mass means a stronger interface coupling effect between two adjacent substructures.

The class diagram of calculating and selecting substructure modes is illustrated in Fig. 4. The method generateSubstructuremodes() in FrequencyAlgo is defined to take charge of the mode calculation and selection. The vibration modes are calculated by generateVibrationmodes() through calling the existing eigenvalue solvers. Meanwhile, the constraint modes are calculated in generateConstraintmodes() through implementing the Guyan reduction method. Two methods selectEMMs() and selectEIMs() are defined in EigenIntegrator to determine the dominant vibration modes of substructures. They are implemented based on the effective modal mass and effective interface mass, respectively.

3.2.2 Assembly of governing equation in hybrid coordinates

The implementation of governing equations in hybrid coordinates involves assembling load vectors and stiffness matrices through the transformation matrix in Eqs. (3) or (5). In the original OpenSees framework, load vectors and stiffness matrices are assembled directly from nodes and elements to the governing equation. For the AMOR analysis, the load vectors and stiffness matrices are assembled through multiplication by the transformation matrix. The model order reduction is conducted during the coordinate space transformation process. The load vectors and stiffness matrices of substructures that behave elastically are condensed, while remain in the original form for substructures that behave plastically. As a result, the linear substructures in any phase and nonlinear substructures in residual-elastic phase are simulated in modal coordinates, and the nonlinear substructure in plastic-hardening phase are simulated in physical coordinates.

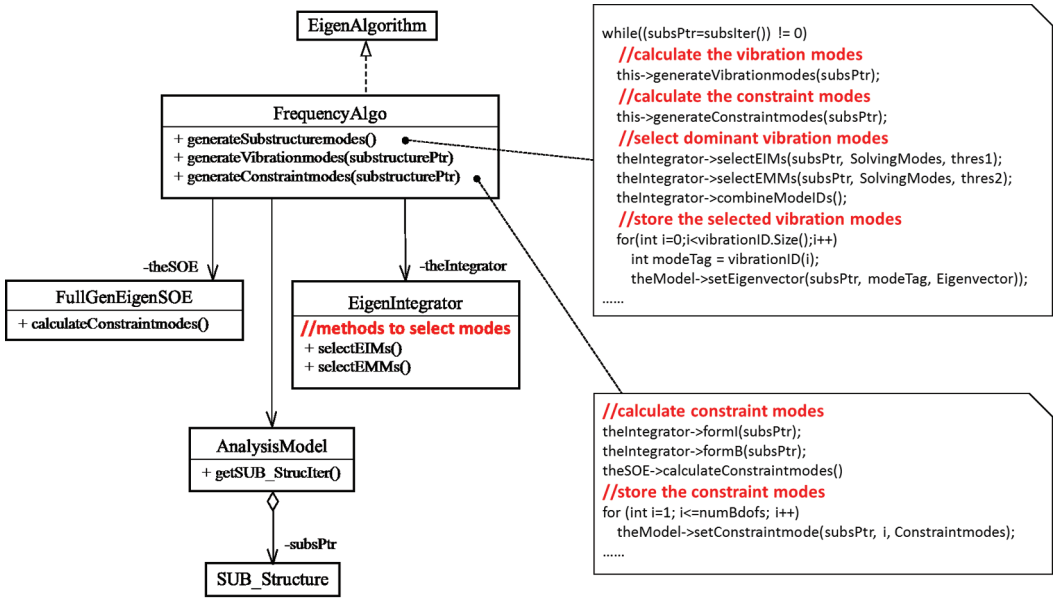

Figure 4: Class diagram of calculating and selecting modes

The class diagram of assembling the governing equation is illustrated in Fig. 5. The assembly of governing equations are conducted through iterating each SUB_Structure object by the methods formSubTangent() and formSubUnbalance(). The methods addSubA() and addSubB() are defined in FullGenLinSOE in charge of assembling the load vectors and tangent matrices of governing equations. For linear substructures in any phase and nonlinear substructures in residual-elastic phase, the governing equations are assembled through the transformation matrix that is accessed in the SUB_Structure object. While for the nonlinear substructure in plastic-hardening phase, the DOF_Group and FE_Element objects contribute to the governing equations directly in their original manner.

3.3 AMOR analysis

The implementation of AMOR analysis involves the reanalysis ability to achieve time-varying substructure modeling according to the gradually changing structural damage distribution. When the damage states of structural components change at a time step τ, the trial solution of governing equations at the time step τ will be eliminated, and the time history analysis turns back to the time step $\tau - \Delta t$. A reanalysis step is required here to proceed the time history analysis based on an updated substructure modeling pattern. The procedure of reanalysis is as follows:

Step 1: The displacement vectors of the entire structure is transformed from the hybrid coordinate space to the physical coordinate space. The partition pattern of all the substructures is updated according to the renewed damage distribution, which results in divided displacement sub-vectors.

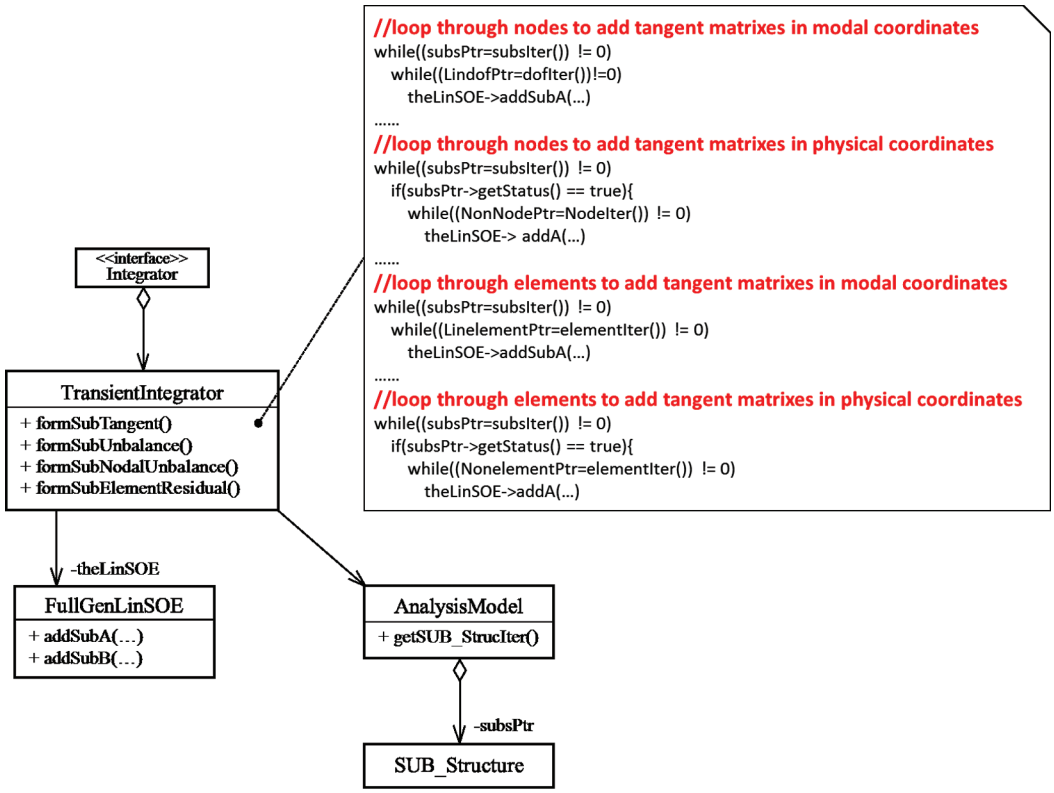

Figure 5: Class diagram of forming governing equations in hybrid coordinates

Step 2: Vibration modes and constraint modes are calculated and the vibration modes are selected for substructures. Thus a transformation matrix is formed by those substructure modes. The governing equation is assembled through this transformation matrix at the time step τ, and re-solved by the existing solver in OpenSees.

Step 3: The displacement vectors of the governing equation at the time step τ will be committed and proceed to the next time step $\tau+\Delta t$, if the damage state of structural components at the time step τ remains unchanged from the time step $\tau-\Delta t$. Otherwise, it's determined to abandon the trial solution and go to the Step 1.

The sequence diagram of the AMOR analysis is illustrated in Fig. 6. The analyze() is the most important method, which advances the analysis state of the FE model with the substructure-based model order reduction, and conducts a reanalysis when the damage state of structural components changes. Once the damage state of structural components is updated, the analyze() invokes modelChange() to call partitionSubs() in AnalysisModel to partition substructures, and call number_Substructures() and number_Equations() in DOF_Numberer to map substructure DOFs and governing equations. Afterwards, generateSubstructureModes() and generateTransformationMatrix() in FrequencyAlgo are

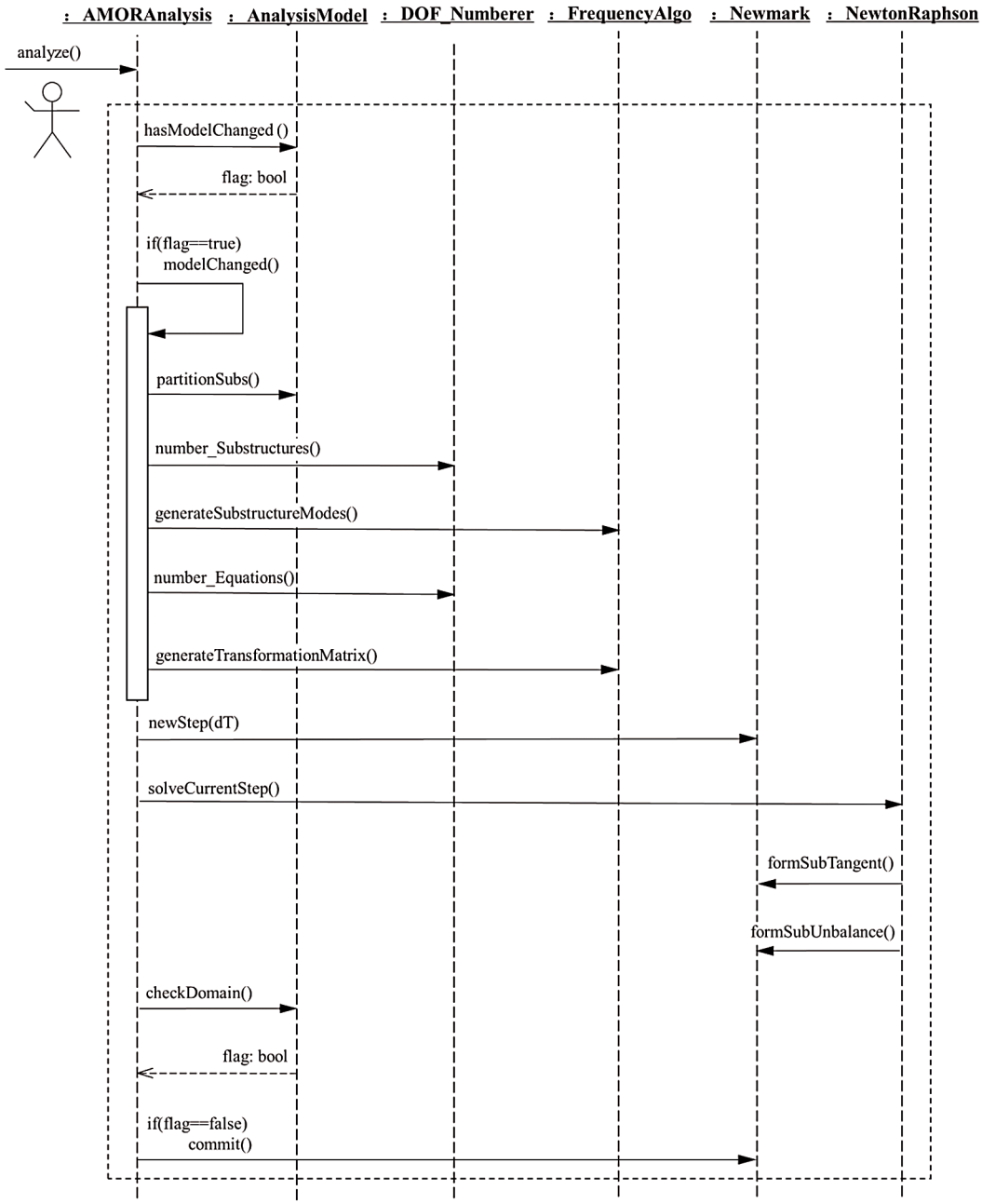

Figure 6: Sequence diagram for the method AMORAnalysis()

invoked to calculate and select substructure modes, and form the coordinate transformation matrix. Subsequently, the analyze() calls the solveCurrentStep() to invoke the methods in Newmark to assemble the governing equations in hybrid coordinates. The governing equations is further solved in method solveCurrentStep() through a number of trail iterations until the convergent solution is found. Only when the damage state of structural components keeps the same status as the previous time step, the displacement solutions will be committed and stored in the domain object.

4 Validation

4.1 Description of the test structure

To test the performance of the AMOR method in OpenSees, a 12-story RC frame structure is employed to conduct the numerical simulation, as shown in Fig. 7. The section information of the RC frame structure is listed in Tab. 1.

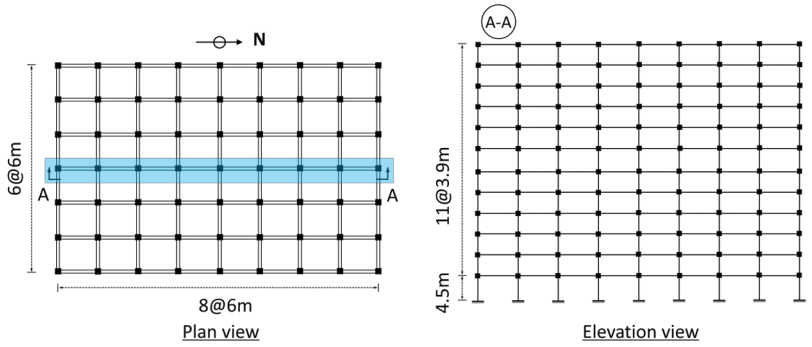

Figure 7: Plan view and elevation view of a 12-story building

Table 1: Section information of a 12-story building

Story	Section dimension (mm×mm)			Reinforcement area (mm^2)		
	Mid-Columns	Side Columns	Beams	Mid-Columns	Side Columns	Beams
1-6	600×600	600×600	300×500	7060	7060	3600
7-12	500×500	500×500	250×500	4930	4930	3000

The two-dimensional model in the load direction is developed in the OpenSees program. All beams and columns of are modeled with 5 fiber-based nonlinear elements. Five integration points are considered in order to trace the onset of the yielding state of the beams and columns. The cross sections of the beams and columns are discretized with 50 fibers. The concrete fiber is modeled using the uniaxial Kent-Scott-Park concrete material model with a degraded linear unloading/reloading stiffness and an assigned tensile strength. The compressive strength of the cover concrete is 30 MPa, and the corresponding strain is

0.002. The compressive strength and compressive strain of the core concrete are determined according to the confined concrete model proposed by Kent and Park. The steel rebar fiber is modeled using the uniaxial bilinear steel material model with kinematic hardening. The yield strength of the longitudinal rebar in the beams and columns is 400 MPa. The Young's modulus and strain-hardening ratio of the longitudinal rebar are 200 GPa and 0.01, respectively. The first three periods of the structure are 1.83 s, 0.63 s and 0.35 s. The Rayleigh damping is employed in the nonlinear seismic analysis.

The acceleration records from the El Centro, Kobe, Northridge and Parkfield earthquakes are employed as earthquake inputs. The peak ground accelerations (PGA) of these records are scaled from 100 gal to 500 gal. The time histories of these acceleration records are normalized and shown in Fig. 8. And the information of these earthquake records are summarized in Tab. 2.

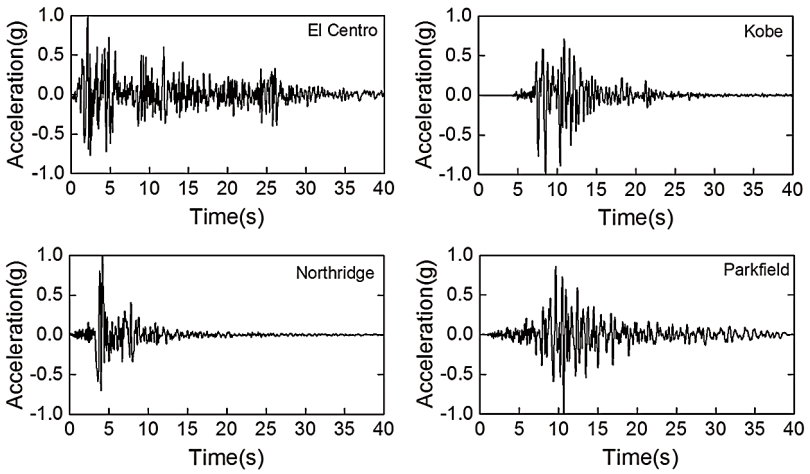

Figure 8: Time histories of the normalized earthquake records

Table 2: Information of earthquake records

Event	Station name	Magnitude (Mw)	Depth (km)	ID in this paper
Imperial Valley	El Centro Array #9	6.95	15.69	El Centro
Kobe, Japan	Fukushima	6.90	47.11	Kobe
Northridge	Beverly Hills	6.69	23.89	Northridge
Parkfield	Cholame	6.00	14.02	Parkfield

The results of nonlinear time history analysis are taken for assessing the accuracy and efficiency of the AMOR method in OpenSees. All examples are run on a PC workstation that is equipped with an Intel Xeon E5-2640 CPU @ 2.4 GHz processor and 64 GB of RAM.

4.2 Seismic response of the test structure

The seismic response of the test structure is simulated by both the conventional time step integration (TSI) method and AMOR method in OpenSees. The simulation results are compared to validate the performance of the AMOR method in OpenSees. The story-drift ratios of the test structure under seismic excitations with PGAs from 100 gal to 500 gal are shown in Fig. 9. Moreover, the time histories of roof displacement under seismic excitation with a PGA of 500 gal is shown in Fig. 10. The seismic response of the AMOR method agrees well with that of the TSI method. To compare the localized nonlinearity, Fig. 11 plots the moment-rotation curves of a beam element that enter nonlinear stage under earthquakes with a PGA of 500 gal. The moment-rotation curves of the AMOR method and the TSI method are also consistent with each other.

To quantitatively measure the accuracy of the AMOR method and the TSI method, the average relative errors of the story-drift ratio curves are summarized in Tab. 2. The maximum errors of story-drift ratio for El Centro, Kobe, Northridge, and Parkfield are approximately 2.76%, 5.15%, 3.47%, and 3.96%, respectively. The simulation error mainly comes from two aspects. Firstly, the trigger of elastic and plastic state of the curved concrete constitute model is set as the half of the yield stress, which may induce minor simulating errors. Secondly, the response of substructure in modal coordinate space is represented by a number of low-order modes, and the ignorance of high-order modes introduces additional simulation errors. However, the simulation errors listed in Tab. 3 are quite small and acceptable.

4.3 Model order reduction and computational time

The effectiveness of the AMOR method mainly depends on the characteristics of initial-elastic phase and residual-elastic phase. When the duration of these two states is longer and the switching frequency of different damage states is lower, the AMOR method may have a better MOR effect. That's because the longer duration of initial-elastic phase provides a larger number of time intervals, in which the model order reduction for the entire structure is available. And the longer duration of residual-elastic phase facilitates the model order reduction for the nonlinear substructures. On the other side, the lower switching frequency of different damage states limits the additional computational time required for modeling substructures and updating governing equations.

Fig. 12 shows the time history curves of the three types of damage state when the test structure is excited by four earthquakes with various intensities. The symbols "i", "p" and "e" stand for three damage states, i.e., the initial-elastic phase, the plastic-hardening phase, and the residual-elastic phase, respectively. A set of three numbers in a bracket stands for the ratios of the duration of three damage states to the ground motion duration. The alternation of different damage states can be clearly observed in time history curves. As the ground motion intensity increases, the duration of initial-elastic phase and residual-elastic phase decreases and the switching frequency increases. Since the duration of these two damage states for all earthquake records are longer than the 80% of seismic

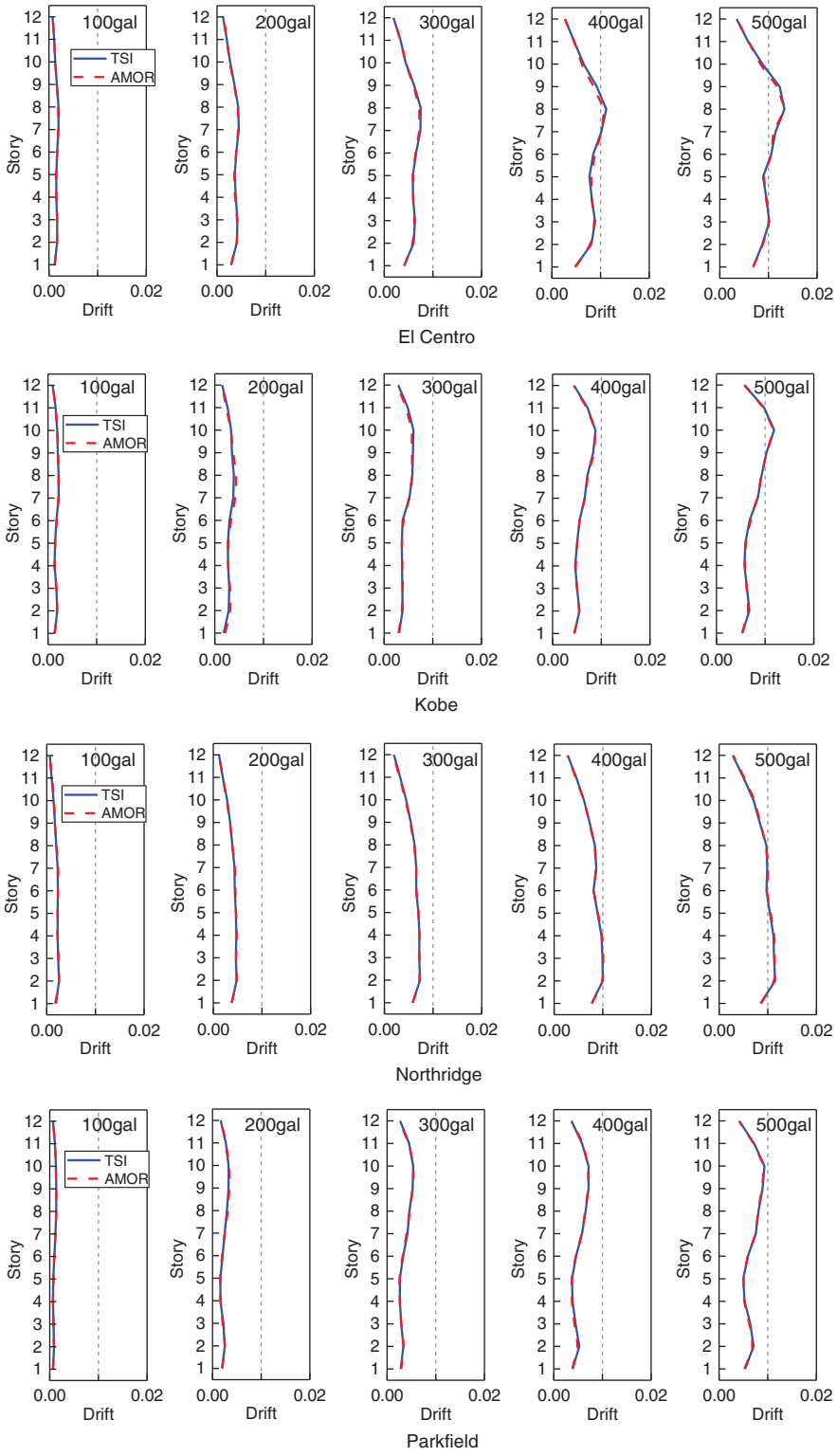

Figure 9: Time histories of the normalized earthquake records

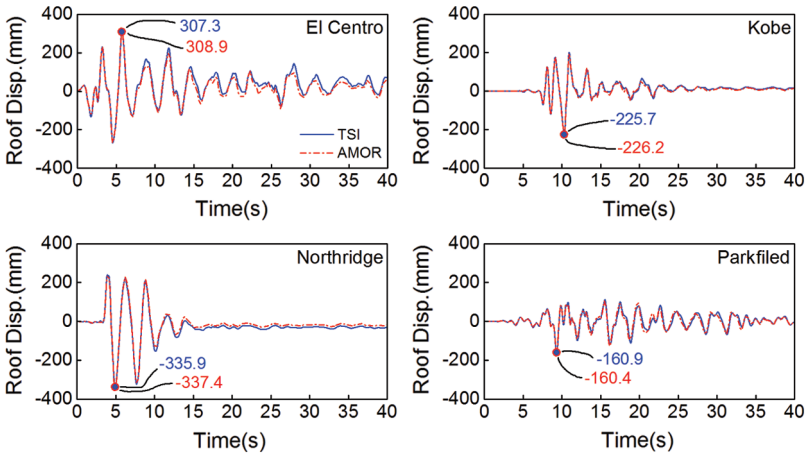

Figure 10: Time history of roof displacements (PGA=500 gal)

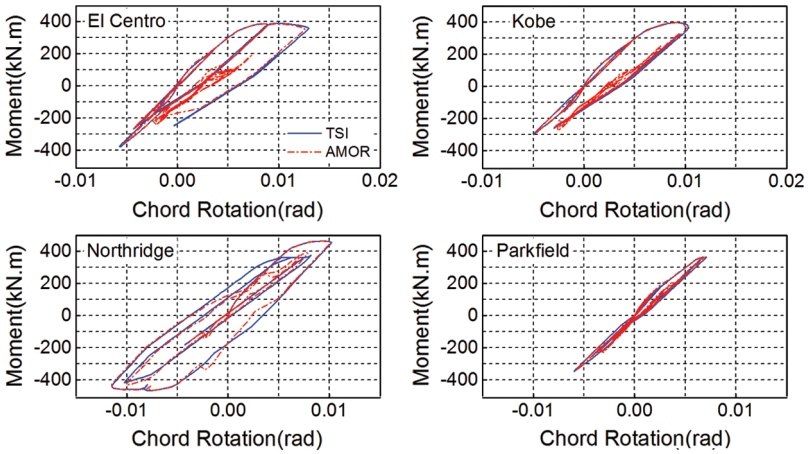

Figure 11: Moment-rotation curves (PGA=500 gal)

loading period. The AMOR has a great potential to make model order reduction for nonlinear seismic analysis.

The number of DOFs in the AMOR method is suitable to assess the efficiency of the model order reduction. This study set the DOF reduction ratio as the ratio of hybrid DOFs in the AMOR method to the DOFs of the non-reduced model. Fig. 13 describes the DOF reduction ratio of the test structure simulated by AMOR under four earthquakes with a PGA of 500 gal. It can be clearly seen that the AMOR generates a DOF reduction ratio of around 0.01 and makes a remarkable model order reduction during the initial-elastic period and the residual-elastic period. For the plastic-hardening period, the DOF reduction ratio approximately ranges from 0.24 to 0.77. Because of the long duration of the

Table 3: Average errors of the story drift ratio curves (%)

Ground motion intensity (gal)	Seismic input records			
	El Centro	Kobe	Northridge	Parkfield
100	1.70	2.73	3.47	2.26
200	2.76	5.15	1.46	3.96
300	1.59	3.23	1.46	2.57
400	2.60	0.88	1.12	2.47
500	2.07	1.13	1.64	1.62

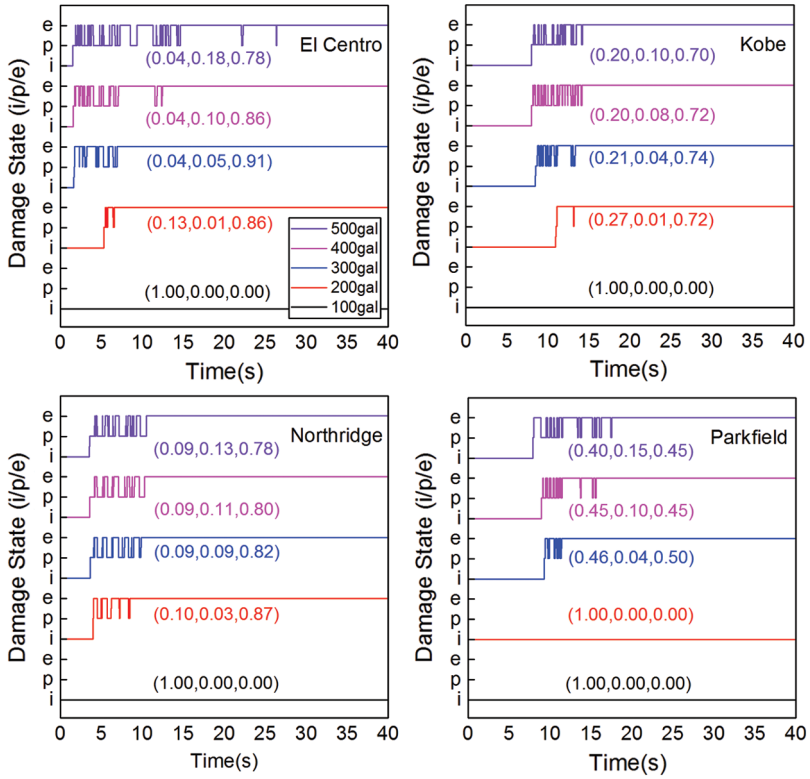

Figure 12: Time histories of the three types of damage state

initial-elastic phase and residual-elastic phase, the model order reduction for all four earthquake records is substantially effective.

The advantage of the AMOR method is to minimize the number of DOFs of governing equations during different damage states, so as to accelerate the solving process of

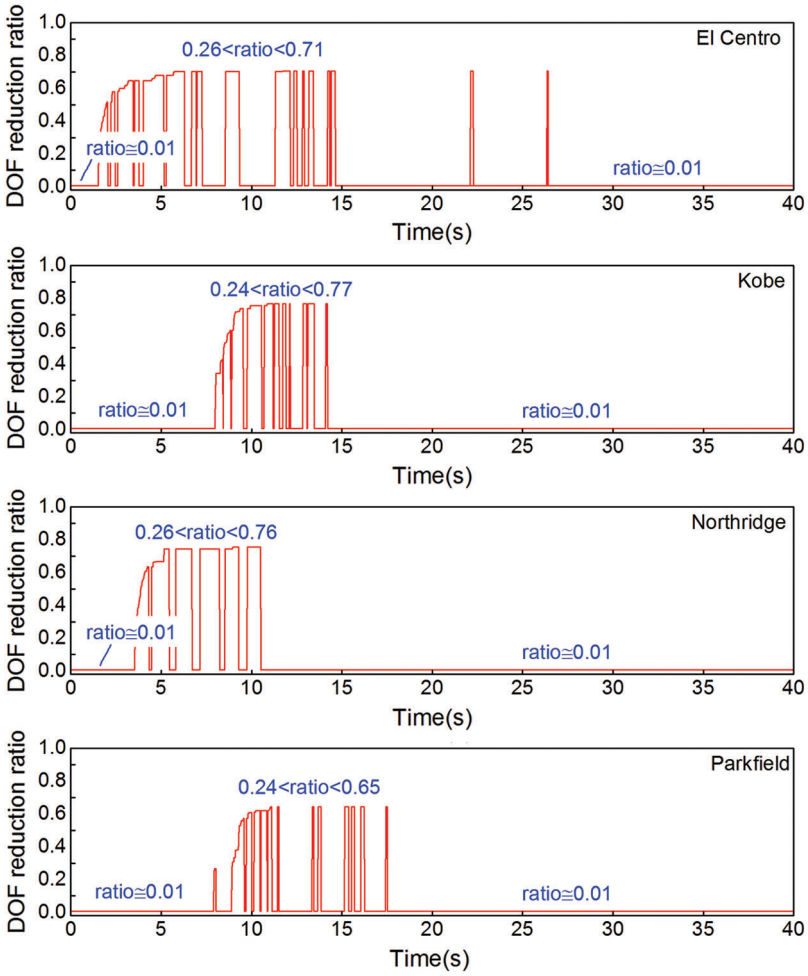

Figure 13: Time history of DOF reduction ratio (PGA=500 gal)

equations. This investigation compares the simulation time of the AMOR with that of the TSI, as shown in Fig. 14. The ratios of the simulation time are also summarized in Tab. 4. When the ground motion intensity is as low as 100 gal, the entire structure keeps in initial-elastic phase throughout the seismic loading period. The seismic response of the test structure is simulated by a small number of vibration modes. And the ratio of simulation time between AMOR and TSI ranges from 30% to 35%. When the ground motion intensities increase, the test structure enters residual-elastic phase during the attenuating period of seismic loads. The model order reduction of nonlinear substructures makes a significant contribution to the solving speed of governing equations. Thus the ratio of simulation time between AMOR and TSI is reduced to about 40%~60% of TSI.

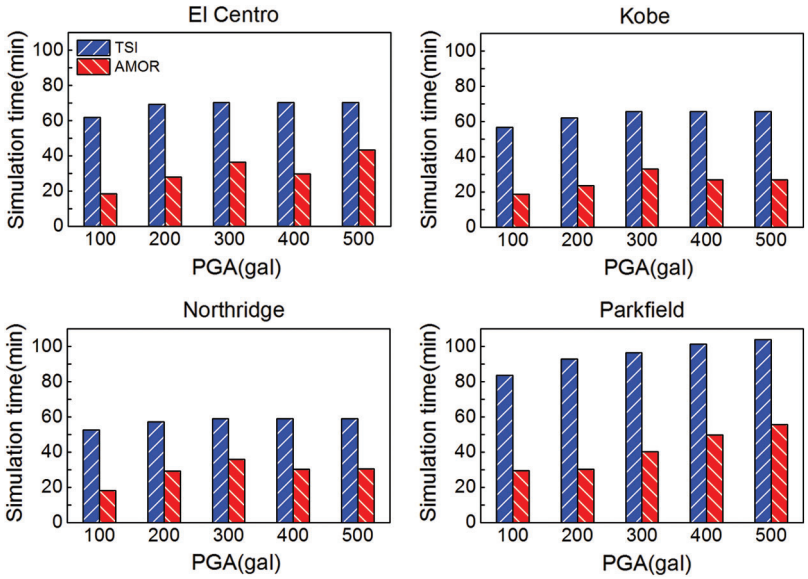

Figure 14: Comparison of the simulation time

Table 4: Ratio of the simulation time

Ground motion intensity (gal)	Seismic input records			
	El Centro	**Kobe**	**Northridge**	**Parkfield**
100	0.30	0.33	0.35	0.35
200	0.40	0.38	0.51	0.33
300	0.52	0.50	0.61	0.42
400	0.42	0.41	0.51	0.49
500	0.61	0.41	0.52	0.53

It's been observed that the AMOR method has an improved performance in simulation efficiency when compared to the TSI method.

5 Conclusions

In this paper, an adaptive substructure-based model order reduction method (AMOR) is developed, which generates time-varying substructures and makes model order reduction for substructures in the initial-elastic phase, the plastic-hardening phase and the residual-elastic phase, respectively. The finite-element software framework OpenSees is extended to perform the AMOR analysis through implementing a substructure layer of abstraction and a transient analysis class. The capacity of the AMOR method and its implementation are tested using a 12-story reinforced concrete frame structure. Acceptable agreements of

the seismic response are achieved between the conventional time step integration (TSI) method and the AMOR method. The advanced software architecture is validated to be able to generate time-varying substructures and reduce substructure DOFs in different damage phases. The simulation efficiency of the AMOR method is higher than the TSI method. The long duration of the initial-elastic phase and residual-elastic phase increases the AMOR's efficiency, while the high switching frequency of different damage phases decreases the AMOR's efficiency. In the future work, the influence of the switching frequency should be eliminated to further reduce the computational time.

Funding Statement: This work is supported by the National Nature Science Foundation of China (No. 51678210) and National Key Research and Development Program of China (No. 2016YFC0701400).

Conflicts of Interest: The authors declare that they have no conflicts of interest to report regarding the present study.

References

ABAQUS (2019): *Abaqus Analysis User's Manual*. Version 6.19. Simulia Inc., Providence.

ANSYS (2019): *User's Manual*. Version 19.0. Swanson Analysis Systems Inc., Houston.

Aguado, J. V.; Chinesta, F.; Leygue, A.; Cueto, E.; Huerta, A. (2013): DEIM-Based PGD for parametric nonlinear model order reduction. *6th International Conference on Adaptive Modeling and Simulation (ADMOS)*, pp. 29-37. Lisbona, Portugal.

Amsallem, D.; Zahr, M. J.; Farhat, C. (2012): Nonlinear model order reduction based on local reduced-order bases. *International Journal for Numerical Methods in Engineering*, vol. 92, no. 4, pp. 891-916. DOI 10.1002/nme.4371.

Bampton, M. C. C.; Craig, J. R. R. (1968): Coupling of substructures for dynamic analyses. *AIAA Journal*, vol. 6, no. 7, pp. 1313-1319. DOI 10.2514/3.4741.

Capaldo, M.; Guidault, P. A.; Néron, D.; Ladevèzeb, P. (2017): The reference point method, a "hyperreduction" technique: application to PGD-based nonlinear model reduction. *Computer Methods in Applied Mechanics and Engineering*, vol. 322, pp. 483-514. DOI 10.1016/j.cma.2017.04.033.

Carlberg, K.; Farhat, C.; Cortial, J.; Amsallem, D. (2012): The GNAT method for nonlinear model reduction: effective implementation and application to computational fluid dynamics and turbulent flows. *Journal of Computational Physics*, vol. 242, pp. 623-647. DOI 10.1016/j.jcp.2013.02.028.

Chatterjee, A. (2000): An introduction to the proper orthogonal decomposition. *Current Science*, vol. 78, pp. 808-817.

Chaturantabut, S.; Sorensen, D. C. (2010): Nonlinear model reduction via discrete empirical interpolation. *SIAM Journal on Scientific Computing*, vol. 32, no. 5, pp. 2737-2764. DOI 10.1137/090766498.

Chinesta, F.; Ammar, A.; Cueto, E. (2010): Recent advances and new challenges in the use of the proper generalized decomposition for solving multidimensional models. *Archives of Computational Methods in Engineering*, vol. 17, no. 4, pp. 327-350. DOI 10.1007/s11831-010-9049-y.

Corigliano, A.; Dossi, M.; Mariani, S. (2015): Model order reduction and domain decomposition strategies for the solution of the dynamic elastic-plastic structural problem. *Computer Methods in Applied Mechanics and Engineering*, vol. 290, pp. 127-155. DOI 10.1016/j.cma.2015.02.021.

Fang, M.; Wang, J.; Li, H. (2018): An adaptive numerical scheme based on the Craig-Bampton method for the dynamic analysis of tall buildings. *Structural Design of Tall and Special Buildings*, vol. 27, no. 1, pp. 1410-1423. DOI 10.1002/tal.1410.

Farhat, C.; Avery, P.; Chapman, T.; Cortial, J. (2014): Dimensional reduction of nonlinear finite element dynamic models with finite rotations and energy-based mesh sampling and weighting for computational efficiency. *International Journal for Numerical Methods in Engineering*, vol. 98, no. 9, pp. 625-662. DOI 10.1002/nme.4668.

Gamma, E.; Helm, R.; Johnson, R.; Vlissides, J. (1995): *Design Patterns: Elements of Reusable Object-Oriented Software*. Addison-Wesley, Reading, Massachusetts.

Gu, Q.; Wang, L.; Huang, S. R. (2019): Integration of peridynamic theory and OpenSees for solving problems in civil engineering. *Computer Modeling in Engineering & Sciences*, vol. 120, no. 3, pp. 471-489. DOI 10.32604/cmes.2019.05757.

Guo, M.; Hesthaven, J. S. (2018): Reduced order modeling for nonlinear structural analysis using Gaussian process regression. *Computer Methods in Applied Mechanics and Engineering*, vol. 341, pp. 807-826. DOI 10.1016/j.cma.2018.07.017.

Guyan, R. J. (1965): Reduction of stiffness and mass matrices. *AIAA Journal*, vol. 3, no. 2, pp. 380. DOI 10.2514/3.2874.

He, H.; Wang, T.; Chen, G. (2016): A hybrid coordinates component mode synthesis method for dynamic analysis of structures with localized nonlinearities. *ASME Journal of Vibration and Acoustics*, vol. 138, no. 3, pp. 031002. DOI 10.1115/1.4032717.

Hesthaven, J. S.; Rozza, G.; Stamm, B. (2016): *Certifed Reduced Basis Methods for Parametrized Partial Differential Equations*. Springer, New York.

Hurty, W. (1963): On the dynamic analysis of structural systems using component modes. *AIAA Journal*, vol. 3, no. 4, pp. 678-685. DOI 10.2514/3.2947.

Huynh, D. B. P.; Knezevic, D. J.; Patera, A. T. (2013a): A static condensation reduced basis element method: approximation and a posteriori error estimation. *ESAIM Mathematical Modelling and Numerical Analysis*, vol. 47, pp. 213-251.

Huynh, D. B. P.; Knezevic, D. J.; Patera, A. T. (2013b): A static condensation reduced basis element method: complex problems. *Computer Methods in Applied Mechanics and Engineering*, vol. 259, pp. 197-216.

Kammer, D. C.; Triller, M. J. (1996): Selection of component modes for Craig-BamptonSubstructure representations. *AIAA Journal*, vol. 118, no. 2, pp. 264-270.

Kerschen, G.; Golinval, J. C. (2002): Physical interpretation of the proper orthogonal modes using the singular value decomposition. *Journal of Sound and Vibration*, vol. 249, no. 5, pp. 849-865. DOI 10.1006/jsvi.2001.3930.

Kerschen, G.; Golinval, J. C.; Vakakis, A. F.; Bergman, L. A. (2005): The method of proper orthogonal decomposition for dynamical characterization and order reduction of mechanical systems: an overview. *Nonlinear Dynamics*, vol. 41, no. 1-3, pp. 147-169. DOI 10.1007/s11071-005-2803-2.

Ladevèze, P.; Passieux, J. C.; Néron, D. (2010): The LATIN multiscale computational method and the proper generalized decomposition. *Computer Methods in Applied Mechanics and Engineering*, vol. 199, no. 21-22, pp. 1287-1296. DOI 10.1016/j.cma.2009.06.023.

Lu, X. Z.; Tian, Y.; Sun, C. J.; Zhang, S. H. (2019): Development and application of a high-performance triangular shell element and an explicit algorithm in OpenSees for strongly nonlinear analysis. *Computer Modeling in Engineering & Sciences*, vol. 120, no. 3, pp. 561-582. DOI 10.32604/cmes.2019.04770.

Lu, X. Z.; Xie, L.; Guan, H.; Huang, Y.; Lu, X. (2015): A shear wall element for nonlinear seismic analysis of super-tall buildings using OpenSees. *Finite Elements in Analysis and Design*, vol. 98, pp. 14-25. DOI 10.1016/j.finel.2015.01.006.

Maday, Y.; Rønquist, E. M. (2002): A reduced-basis element method. *Journal of Scientific Computing*, vol. 1, no. 1, pp. 447-459. DOI 10.1023/A:1015197908587.

Maday, Y.; Rønquist, E. M. (2005): The reduced basis element method: application to a thermal fin problem. *SIAM Journal on Scientific Computing*, vol. 26, no. 1, pp. 240-258. DOI 10.1137/S1064827502419932.

Mckenna, F.; Scott, M. H.; Fenves, G. L. (2010): Nonlinear finite-element analysis software architecture using object composition. *Journal of Computing in Civil Engineering*, vol. 24, no. 1, pp. 95-107. DOI 10.1061/(ASCE)CP.1943-5487.0000002.

Mohamed, K. S. (2018): *Machine Learning for Model Order Reduction*. Springer, New York.

Moosavi, A.; Stefanescu, R.; Sandu, A. (2015): *Efficient Construction of Local Parametric Reduced Order Models Using Machine Learning Techniques*. Computer Science Technical Report CSTR-22.

Nguyen, N. C.; Peraire, J. (2016): Gaussian functional regression for output prediction: model assimilation and experimental design. *Journal of Computational Physics*, vol. 309, pp. 52-68. DOI 10.1016/j.jcp.2015.12.035.

Nouy, A. (2010): A priori model reduction through proper generalized decomposition for solving time-dependent partial differential equations. *Computer Modeling in Engineering & Sciences*, vol. 199, pp. 1603-1626.

Grepl, M. A. (2005): *Reduced Basis Approximation and a Posteriori Error Estimation for Parabolic Partial Differential Equations. (Ph.D. Thesis)*. Massachusetts Institute of Technology, USA.

Quarteroni, A.; Manzoni, A.; Negri, F. (2016): *Reduced Basis Methods for Partial Differential Equations: An Introduction*. Springer, New York.

Rozza, G.; Huynh, D. B. P.; Patera, A. T. (2007): Reduced basis approximation and a posteriori error estimation for affinely parametrized elliptic coercive partial differential equations. *Archives of Computational Methods in Engineering*, vol. 15, no. 3, pp. 1-47. DOI 10.1007/BF03024948.

Ryckelynck, D. (2009): Hyper-reduction of mechanical models involving internal variables. *International Journal for Numerical Methods in Engineering*, vol. 77, no. 1, pp. 75-89. DOI 10.1002/nme.2406.

Sun, B. Y.; Li, S. F.; Gu, Q.; Ou, J. P. (2019): Coupling of peridynamics and numerical substructure method for modeling structures with local discontinuities. *Computer Modeling in Engineering & Sciences*, vol. 120, no. 3, pp. 739-757. DOI 10.32604/cmes.2019.05085.

Vallaghé, S.; Patera, A. T. (2014): The static condensation reduced basis element method for a mixed-mean conjugate heat exchanger model. *SIAM Journal on Scientific Computing*, vol. 36, no. 3, pp. B294-B320. DOI 10.1137/120887709.

Wang, F.; Jiang, N. (2012): 3D dynamic analysis of soil-structure interaction system based on mixed linear-nonlinear substructure method. *Engineering Mechanics (in Chinese)*, vol. 29, no. 9, pp. 155-161. DOI 10.3901/JME.2012.09.155.